Multi-scale investigation of dislocation mediated carbon migration in iron

Tigany Zarrouk

August 8, 2020

Contents

Abstract

We investigate the validity of a dislocation-assisted carbon migration mechanism underpinning the formation of dark etching regions in bearing steels undergoing high-cycle fatigue through use of a multi-scale approach: from quantum mechanics, to stochastic simulations. We start from tight binding simulations of $1/3\langle 111\rangle$ screw dislocations to obtain the 2-d Peierls potential and Fe-C binding energies. These become ingredients for a line-tension model of the $1/3\langle 111\rangle$ screw dislocation to obtain the kink-pair formation energy as a function of stress and carbon concentration. Finally, 3-d kinetic Monte-Carlo simulations of dislocations in an environment of carbon are used to ascertain which temperature and stress regimes dislocation-assisted carbon migration is a valid mechanism.

1 Introduction

- Outline of the literature review
    1. Origin of DER formation through high-cycle fatigue
    2. What is the DER region and what phases is it composed of?
    3. What are the current mechanisms which explain this?

(a) Why are they insufficient?

4. Ouline of the work considering Fe-C dislocation modelling

Martensitic steels are frequently used in bearings due to their resilience to service conditions, such as high rotational speeds and contact pressures. However, under cyclic loading exceeding a given contact stress (the elastic shakedown limit), the microstructure of the steel can decay, signalling the onset of rolling cycle fatigue (RCF), enhancing the risk of failure from subsurface crack initiation. This microstructural decay corresponds to Dark Etching Regions (DERs) as seen in optical images, where the darkness of the images is due to the higher reactivity of the phases which compose the DER region to the etchant, exacerbated by the roughness of the DER region, with more grains per unit area scattering light.

Further development of the DER occurs with more stress cycles (of which development is hastened with a higher contact pressure). Matured DER regions have additional features, such as white etching bands (WEBs), which occur at specific angles (30 deg /80 deg, for low angle / high angle WEBs respectively).

DERs are found in the subsurface of the material, due to the maximum deviatoric stress being found in the subsurface from the Hertzian stress distribution exhibited by bearing contact.

These DER regions are composed of multiple different phases. They are generally defined to be mixtures of ferritic features within a residual martensitic matrix initially, but there are other phases which appear upon the further degredation of martensite during RCF.

There are: ferrite microbands which are generally grouped together; elongated ferrite, which may be composed by multiple ferrite microbands joining together—these have also been seen to form WEBs along with ferrite microbands; residual carbides, in which ferrite (microbands and elongated) can form inside of, causing it to dissolve; lenticular carbides, which are formed on the side and parallel to WEBs, and are observed in conjunction with the formation of WEBs.

It is thought that the formation of lenticular carbides is related to the dissolution of residual cementite and tempered carbides, increasing the carbon content within the the ferrite microbands/nanocrystalline ferrite (DER) and reducing solubility of the carbon within WEBs. Residual cementite does not need to by fully dissolved for the formation of lenticular carbides.

Fu *et al.* have claimed that carbon is redistributed into higher carbon concetrated regions such as cementite and other transition carbides.

- Elucidate on the measurements pertaining to the migration of carbon

Many authors have proposed that carbon plays a crucial role in the formation of the DER regions.

Voskamp suggests that cyclic stresses generate a local rise in temperature, which promotes diffusion of atomic carbon trapped in the martensitic matrix. With diffusion of carbon, dislocations become unpinned, enabling potential slip systems to activate. The unpinned dislocations cause deformation.

Polonsky and Keer propose that the redistribution of the carbon solutes cause the formation of ferrite microbands by cyclic-plastic strain induced softening. Carbon redistribution is caused by the release of carbon trapped by dislocations with the application of stress.

Due to the high dislocation density of martensite, all dissolved carbon is segregated to dislocations—which also pin the dislocations. With applied stress, the dislocations become unpinned and mobile. Dislocations multiply/annihilate; with annihilation, carbon becomes in ordinary solution, which is available to diffuse. This diffusion causes the formation of ferritic microbands. The process of annihilation needs to be understood.

Hedman/Slycke propose that the degradation of the DER can by described by the growth of carbides, where the carbide sized are described by Ostwald ripening, and carbon diffuses both thermally and mechanically by dislocation glide.

Slycke proposes a creep deformation based mechanism which is controlled by vacancies produced by the climb of dislocations.

Fu *et al.* propose that the fundamental mechanism to DER formation is carbon migration under RCF driven by gliding dislocations. Strain generated by pulsating stresses allow dislocations to escape their carbon rich environment. The dislocations, now free, re-attract carbon, allowing the Cottrell atmosphere to reform, subsequently pinning the dislocation. This creates a net carbon flux. But, if carbides were to form in martensite, they should follow the Bagaryatskii/Isaichev orientation relationship. The cementite formed within the DER region, has an irregular shape, which must be due to te incomplete dissolution of residual cementite.

Smelova proposes that the formation of elongated ferrite are the result of recrystallisation processes.

1.1 Mechanisms

There are many proposed mechanisms for DER formation.

Bush proposes that DER formation is governed by an exchange of material between the carbides and the matrix, which is evidenced by the formation of intrusions/extrusions within the microstructure.

Swahn proposes that the transformation mechanisms which lead to the formation of new features in DER are due to the redistribution of carbon present in the initial microstructure, which in solution in the martensite, and due to the dissolution of carbides.

They further detail that initially, stress induced carbon diffusion leads to the diffusion of carbon from the martensitic lattice to the various defects in the material (mainly dislocations). As plastic deformation accumulates, the movement of dislocations creates carbon rich grain boundary-type interfaces.

It is not certain what role and timescale the dissolution of carbides occurs on.

High operating temperatures are known to accelerate DER formation.

In early stage DER formation, there is a high density of ferrite microbands. Later, regions of homogeneous nanocrystalline ferrite (heavily deformed ferrite) are formed in a cell-like structure.

2 Computational Method

- Use tight-binding model of Paxton and Elsaetter [1].
- Generate dislocations using anisotropic elasticity theory.

- Create clusters of dislocations in both easy and hard core configurations.
- Place carbon in octahedral sites around the core
- Calculate corrections (ZPE etc)

3 Results

3.1 Peierls Potential

To determine the Peierls potential, we followed the procedure detailed in Itakura [2]. Quadrupolar arrays of dislocations were constructed by placing dislocations of antiparallel $1/2\langle 111\rangle$ Burgers vectors in an "S" arrangement [3], with initial displacements determined by the anisotropic elasticity solutions. These displacements were modified to be periodic, thereby removing artificial stacking faults which would appear between periodic images after the introduction of the dipole. This was achieved by the subraction of a linear error term from the superposition of displacement fields arising from the dislocations in the simulation cell and its periodic images [4]. To accomodate for the internal stress upon introduction of the dislocation dipole into a simulation cell, an elastic strain was imposed on the cell, resulting in an extra tilt component being added to the cell vectors [3, 4]. Simulation cells were constructed with different initial core positions, which were sampled from the triangular region "EHS" (easy, hard and split) core positions, as detailed in 1. To fix the dislocation positions during relaxation, the three atoms surrounding the easy core, for each dislocation, were fixed during relaxation.

I do not agree with the calculation of the interaction energy between dislocations in Itakura's paper. Their equation is a sum over periodic images, which leads to a problem in the conditional convergence of the interaction energy, as shown by Bulatov and Cai [4]. The equation found in Itakura would clearly depend on the truncation limit for the sum, which they do not specify.

The interaction energy between the dislocation dipole and periodic images should follow the prescription of Bulatov and Cai [4]. In isotropic elasticity, the elastic energy of a single dislocation dipole in an infinite lattice is given by

$$E_{\mathrm{el}}^{\mathrm{inf}} = \frac{\mu b^2}{4\pi} ln(\frac{r}{r_c})$$

The contribution from periodic images to the correction is

$$E_{\mathrm{img}} = E_{\mathrm{el}}(\mathbf{a}, \mathbf{c}_i, r_c) - E_{\mathrm{el}}^{\mathrm{inf}}(\mathbf{a}, r_c)$$

,

where

$$E_{\mathrm{img}=\sum_{\mathbf{R}}' E_{\mathrm{dd}}(\mathbf{R})},$$

where $\mathbf{R}$ is a sum over dislocation dipoles in the periodic images exclusively.

$$E_{\mathrm{dd}}(\mathbf{R}) = \frac{\mu b^2}{2\pi} \ln \frac{|\mathbf{R}|^2}{|\mathbf{R}+\mathbf{a}| \cdot |\mathbf{R}-\mathbf{a}|}$$

"Ghost" dipoles are introduced to account for the conditional convergence of the sum at $\pm\alpha\mathbf{b}$ and $\pm\beta\mathbf{b}$, where $\alpha = \beta = 0.5$.

The Peierls potential can be calculated by subtraction of the interaction energy of the dislocations in the periodic array, from the energy of the easy core configuration, which is the ground-state dislocation core configuration.

$$\Delta E_{\mathrm{P}} = \Delta E^{\mathrm{tbe}} - \Delta E_{\mathrm{INT}}$$

Comparison of 2d Peierls potentials of the $1/2\langle 111\rangle$ screw dislocation between DFT can by found in [2]. Data was interpolated using 2d cubic splines. "E", "H" and "S" correspond to easy, hard and split core positions respectively, with the latter also corresponding to atomic positions. The relative energies between the different core positions is smaller in tight-binding compared to DFT; most notably, the energies. This is an artifact in the model, which has been validated in NEB calculations of the $1/2\langle 111\rangle$ screw dislocation Peierls barrier, as calculated with NEB, is roughly half that when compared to DFT **ref Luke's Thesis**. The split core as seen in tight-binding is reminiscent of EAM potentials, where the split core energy is lower than that of the hard core, *but first, to check that this is so, one must check that the interaction energy between dislocations follows Bulatov and Cai.*

This may be attributed to lack of core electron repulsion, resulting from the sd-iron tight-binding model.

Pos	ΔE_{INT}	ΔE_{tbe}	ΔE_{P}	$\Delta E_{\mathrm{P}}^{\mathrm{DFT}}$
1	0	0	0	0
2	-0.7	7.3	7.9	3.2
3	-1.4	16.0	17.4	19.2
4	-2.0	22.2	24.2	31.1
5	-2.5	24.8	27.4	39.3
6	-3.3	3.0	6.3	11.5
7	-6.5	7.1	13.6	39.9
8	-9.6	13.0	22.6	75.2
9	-12.5	5.4	17.9	108.9
10	-4.8	22.1	26.9	34.8
11	-7.2	18.2	25.4	37.9
12	-9.8	14.0	23.8	60.7
13	-3.8	11.5	15.3	17.6
14	-6.9	15.1	22.0	29.9
15	-4.3	18.6	22.9	39.7

3.2 Hard and easy core relaxations

To determine the binding energy of carbon to dislocations, we used the cluster method; where the simulation cells consist of a circular cluster of atoms, split into two regions, with a single dislocation introduced into the centre by using the anisotropic elasticity solutions. Each of the clusters were centred on the easy or hard core positions. The cluster of atoms was split into two regions: a central region of dynamic atoms with radius R_1, and an annulus of atoms, between R_1 and R_2, which were fixed to the anisotropic elasticity solutions.

Initially, large cells of with $R_1 = 6\sqrt{2}a_{\mathrm{bcc}}$, and $R_2 = 7\sqrt{2}a_{\mathrm{bcc}}$ and depth of single burger's vector, were relaxed for both the easy and hard cores, which

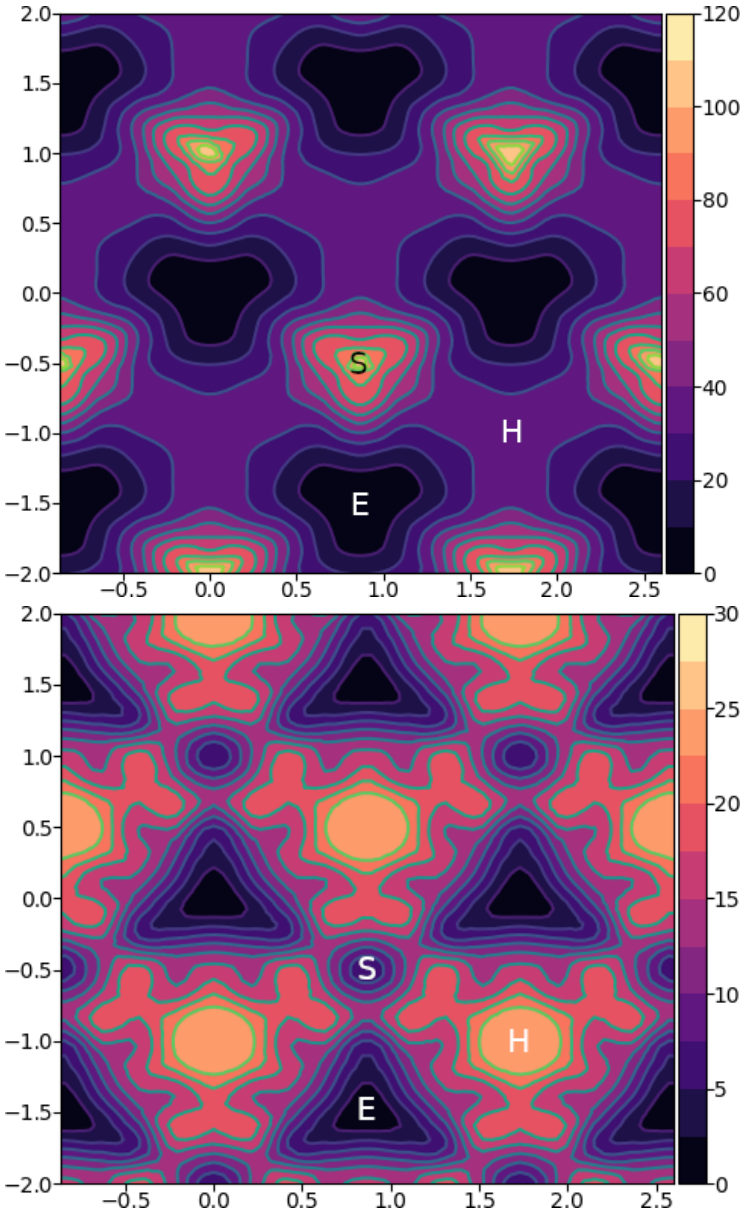

Table 1: Comparison of 2d Peierls potentials of the $1/2\langle 111\rangle$ screw dislocation between DFT cite:Itakura2012 (top) and tight-binding (bottom). Data was interpolated using cubic splines. Energies are in meV, with x and y scales in units of $\sqrt{2}a_{\mathrm{bcc}} = 2\sqrt{2/3}b$. "E", "H" and "S" correspond to easy, hard and split core positions respectively, with the latter also corresponting to atomic positions. The relative energies between the different core positions is smaller in tight-binding compared to DFT. The split core as seen in tight-binding is reminiscent of EAM potentials, where the split core energy is lower than that of the hard core. Some of this discrepancy can be attributed to the difference in simulation method: the cluster method may inhibit the relaxation of the core more than quadrupolar cells, due to finite size effects.

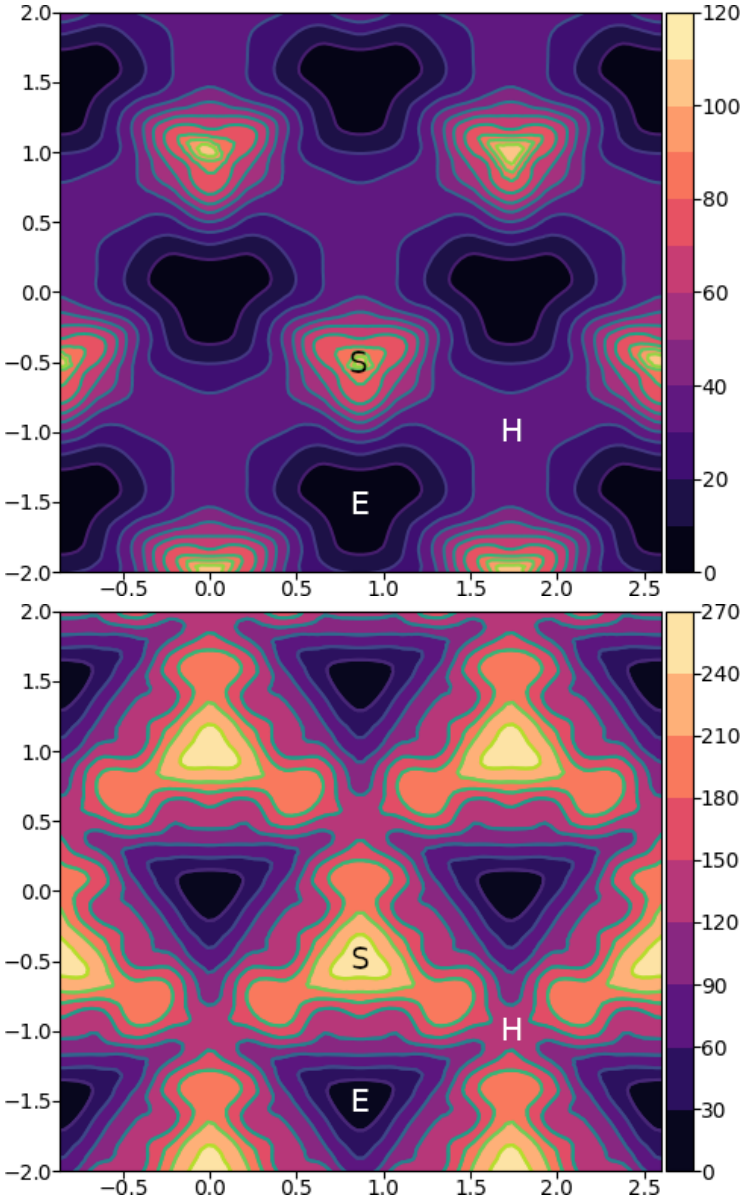

Table 2: Comparison of 2d Peierls potentials of the $1/2\langle 111\rangle$ screw dislocation between DFT cite:Itakura2012 (top) and tight-binding (bottom). Data was interpolated using cubic splines. Energies are in meV, with x and y scales in units of $\sqrt{2}a_{\mathrm{bcc}} = 2\sqrt{2/3}b$. "E", "H" and "S" correspond to easy, hard and split core positions respectively, with the latter also corresponting to atomic positions. The relative energies between the different core positions is smaller in tight-binding compared to DFT. The split core as seen in tight-binding is reminiscent of EAM potentials, where the split core energy is lower than that of the hard core. Some of this discrepancy can be attributed to the difference in simulation method: the cluster method may inhibit the relaxation of the core more than quadrupolar cells, due to finite size effects.

consisted of 522 and 540 atoms respectively. The three atoms surrounding the core were constrained, to only relax in $X-Y$ plane, to stop the core from moving upon relaxation. The k-point sampling mesh for each of these cells was 1x1x24, with a charge tolerance for self-consistency of $1e-6$. Atoms were relaxed until the force on each atom was less than $1e-3$ eV/Å.

From the relaxed cells, a smaller region of 174 atoms, with $R_1 = 3\sqrt{2}a_{\mathrm{bcc}}$, and $R_2 = 4\sqrt{2}a_{\mathrm{bcc}}$, was cut from the dynamic regions. This smaller cell was extended to a thickness of 3b in the Z direction. Carbon interstitials were inserted into octahedral sites near the dislocation core, in the middle layer. Exploiting reflection and rotational symmetry, allows us to use only 10 interstitial sites to obtain the binding energies of carbon ~ 1.8 b from the core.

The three atoms surrounding the core in the first and third layers were again constrained to relax only in the X and Y directions. No such constraints were imposed on the middle layer.

The core energy difference can be estimated by the difference between the excess energies of the easy and hard cores in the limit that $\ln\frac{R}{R_0}) \to 0$. At the smallest value, one finds that the core energy difference $\Delta E_c^{\text{Easy-Hard}} = 76$ meV/b. This is in agreement with the results of Itakura [2], of 82 meV/b.

As found in DFT simulations by Ventelon [5], when a carbon was placed in the vicinity of a relaxed easy dislocation core—in either of the two nearest, distinguishable, octahedral sites—a spontaneous reconstruction of the dislocation core occurred: from easy to hard. Upon reconstruction, the dislocation core moved to a neighbouring triangle, when looking along the $\langle 111 \rangle$ direction, where the carbon found itself situated in the centre.

Plot of dislocation energy as function of cluster size.

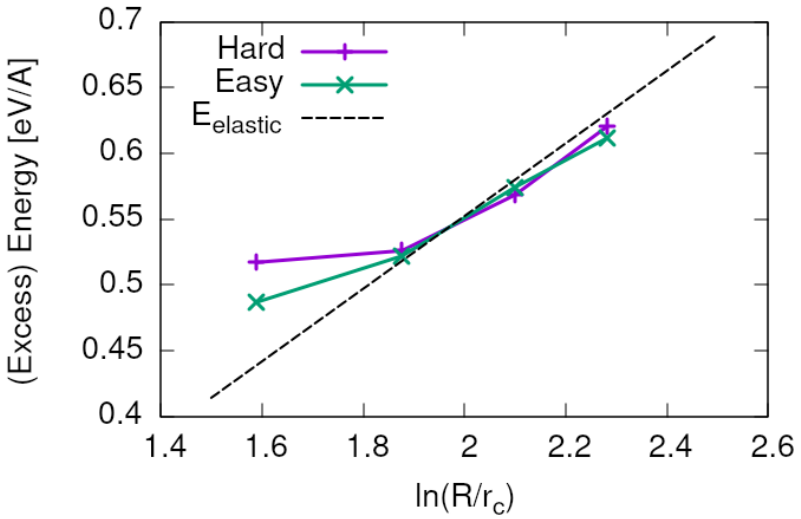

Following the paper by Itakura [6] we calculated the binding energy of carbon each of the screw dislocation cores.

The solution energy is given by

$$E_s = E_{\mathrm{d}\,+\,\mathrm{C}} - E_{\mathrm{d}} - E_{\mathrm{C\ ref.}},$$

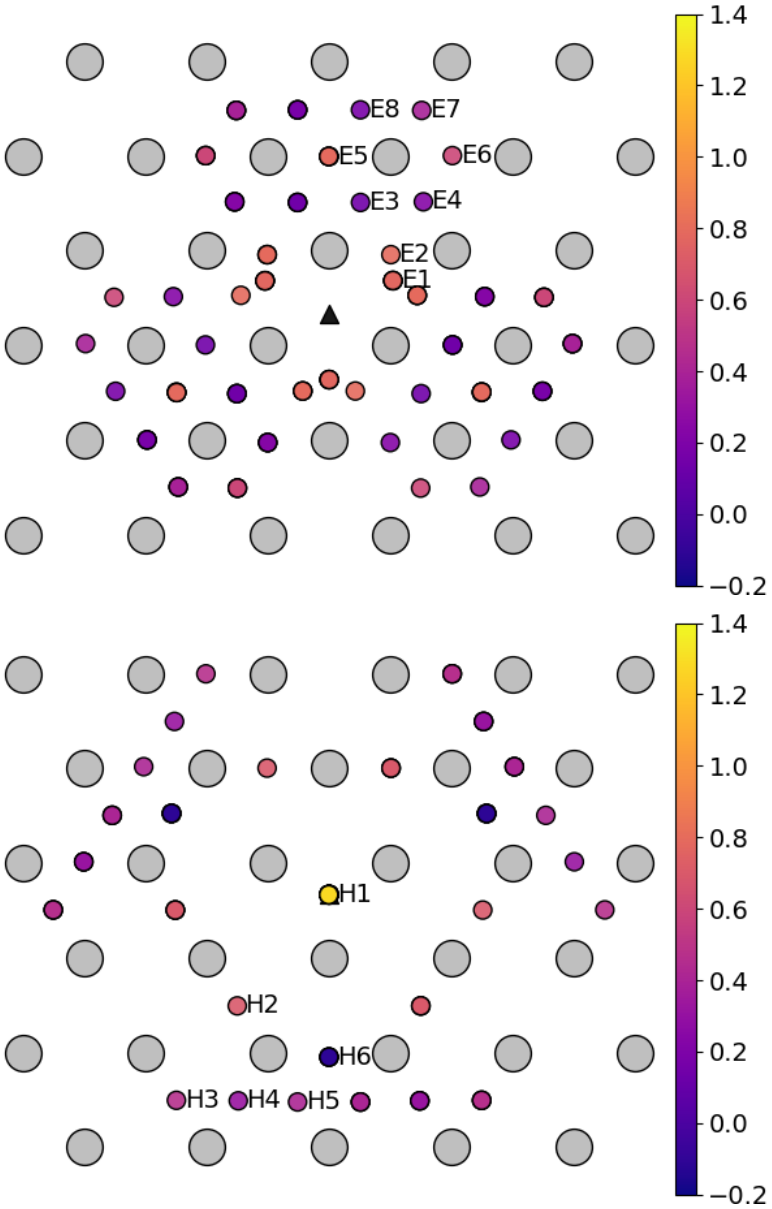

Table 3: Final positions and binding energies (eV) of carbon around the easy core (top) and hard core (bottom). The core was constrained by fixing the top and bottom three atoms surrounding each of the cores. As shown by Ventelon cite:Ventelon2015, the first and second closest octahedral sites to the hard core have their minimum energy inside the hard core.

Site Type	distance from core [b]	E^z [eV]	ΔE^z [eV]	E_b [eV]	E_b^z [eV]
E1	0.57	0.185	-0.018	0.793	0.775
E2	0.70	0.202	-0.001	0.793	0.793
E3	0.99	0.205	0.002	0.137	0.139
E4	1.21	0.208	0.005	0.229	0.234
E5	1.36	0.210	0.008	0.784	0.791
E6	1.66	0.209	0.007	0.597	0.603
E7	1.89	0.206	0.003	0.385	0.388
E8	1.77	0.203	0.000	0.177	0.178
H1	0.00	0.196	-0.006	1.298	1.291
H2	1.19	0.210	0.007	0.691	0.698
H3	2.12	0.209	0.007	0.461	0.467
H4	1.91	0.207	0.005	0.311	0.316
H5	1.80	0.208	0.006	0.403	0.409
H6	1.40	0.207	0.005	-0.119	-0.114

Table 4: Table of energies leading to the zero-point energy corrected binding energy.

where $E_{\mathrm{d}\ +\ \mathrm{C}}$ is the total energy of a relaxed cluster with a carbon interstitial and a dislocation, E_{d} is the total energy of a relaxed cluster with a dislocation and $E_{\mathrm{C\ oct.}}$ is the total energy of relaxed a cluster with a single carbon in an octahedral site.

The zero-point energy is calculated as in Itakura. After relaxation of the C-dislocation system, a 3x3 Hessian matrix is constructed by taking the numerical derivative of forces observed on the carbon atom after displacement by ± 0.015 in each of the X, Y and Z directions. The three atoms surrounding the core on the first and third layers were again fixed in Z coordinate. The zero-point energy is given by

$$E_z = \frac{1}{2}\sum_{i=1}^{3}\frac{h}{2\pi}\sqrt{k_i/m_{\mathrm{C}}},$$

where k_i are the eigenvalues of the Hessian and m_{C} is the mass of carbon.

The ZPE corrected solution energy is given by

$$E_s^{\mathrm{Z}} = E_s + \Delta E_z,$$

where $\Delta E_z = E_z - E_{z\mathrm{C\ ref.}}$ and $E_{z\mathrm{C\ ref.}} = 202.5meV$ is the zero-point energy of carbon situated in an octahedral site in a perfect cluster of the same size.

These binding energies agree well with experiment and previous calculations. The maximum binding energy found by the Fe-C EAM potential by Becquart [7], was 0.41eV. Kamber *et al.* found a maximum binding energy of 0.5 eV. Cochardt found a value of 0.71 eV, which is within 0.1eV of the largest binding energy for the easy core.

EAM calculations by Clouet [8] found a binding energy of —- by calculating the elastic dipole tensor within Eshelby theory. Hanlumyuang *et al.* [9] conducted DFT calculations for the interaction energy 12Å from the core, and their calculations agreed with the continuum limit of Eshelby theory with —-.

In work by Ventelon [5], the interaction energy of a carbon in a hard core prism configuration was found to be 0.79eV for a thickness in the Z direction of

$3b$ (0.73eV for $6b$)—in the convention that a positive binding energy indicates attraction. This is significantly lower than the 1.29eV interaction energy of tight-binding. This discrepancy can be partially explained due to the short cutoff of the carbon interactions in tight-binding—at $\sim a_{\mathrm{bcc}} = 2.87$. In addition, these cells are not fully relaxed, as the three atoms around the core are fixed in Z. As the carbon is separated from its periodic image by $3b = 8.61$, there is no contribution from the repulsive C-C interaction from periodic images, which is included within DFT.

In the mean-field model of Ventelon, we have

$$E_{\mathrm{int}}(c_d) = E_{\mathrm{int}}^{(0)} + \frac{\Delta E_{\text{Easy-Hard}}}{c_d} + c_d V_{\mathrm{CC}},$$

where V_{CC} is the C-C interaction energy which can be found by the equation. In tight-binding $V_{\mathrm{CC}} = 0$,

Distance dependence of binding energies.

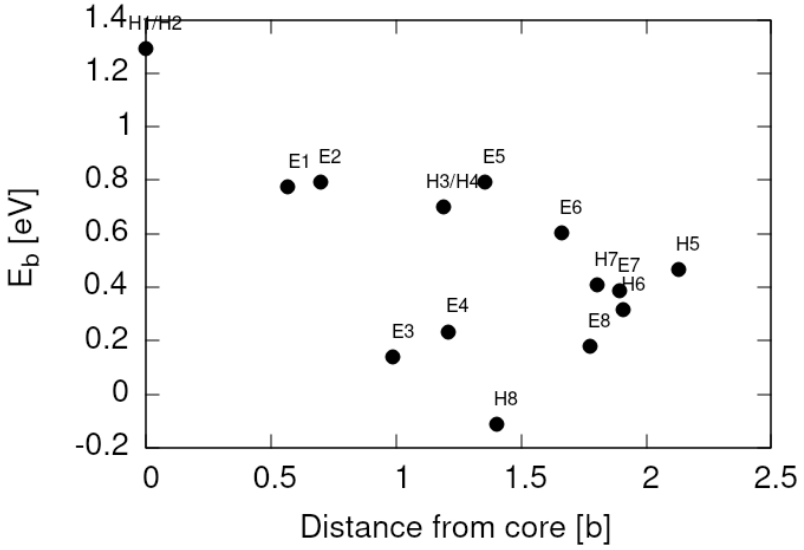

3.3 Line Tension

One is still doing the work for the line tension model. This model views the dislocation as an elastic string which moves on the Peierls potential ΔE_{P}. One is using the julia implementation of the NEB algorithm by Ortner [10]. The equilibrium line shape $y(x)$ of the dislocation is the solution to the 1D Klein-Gordon type equation [11]:

$$-\frac{\mathrm{d}(\Delta E_{\mathrm{P}}[y(x)])}{\mathrm{d}y(x)} + \sigma_{\mathrm{A}} b + T\frac{\partial^2 y}{\partial x^2} = 0,$$

where,

$$T = E_L + \frac{\mathrm{d}^2 E_L}{\mathrm{d}\phi^2},$$

$$E_L = E_{\text{el}} + E_{\text{core}} = \frac{\mu b^2}{2\pi} \ln\left(\frac{R}{r_c}\right) + E_{\text{core}}.$$

I have calculated the coefficients necessary for the line tension model. But there seem to be differences between what Itakura states in his paper and the coefficients that are measured in the Proville paper [11].

One thing I can do to check the coefficients are correct, is to fit to the the kink shape from Luke's thesis to obtain the correct value for the line-tension T.

4 Discussion

- How do the results of this work feed into C migration with dislocations?
- How valid is the theory we have vs Fu *et al.*
-

5 Future work

- Validation of line-tension model by reproduction of the dislocation line shape from Itakura 2012 [2].
- Compare tbe dislocation line shape with Itakura, and find the migration path of the dislocation from tbe data.
- [Optional] Find the elastic dipole tensor to check the binding energy of C within anisotropic elasticity.
- Choose the sites for which one can fit a function (lorentzian) for the interaction energy between C and Fe.
- Find the kink-pair formation enthalpy, with and without carbon, to feed into the kMC code.

6 Bibliography

References

[1] A. T. Paxton and C. Elsässer. Analysis of a carbon dimer bound to a vacancy in iron using density functional theory and a tight binding model. *Physical Review B*, 87(22), June 2013.

[2] M. Itakura, H. Kaburaki, and M. Yamaguchi. First-principles study on the mobility of screw dislocations in bcc iron. *Acta Materialia*, 60(9):3698–3710, May 2012.

[3] Emmanuel Clouet. Screw dislocation in zirconium: An ab initio study. *Physical Review B - Condensed Matter and Materials Physics*, 86(14):1–11, 2012.

[4] Vasily Bulatov. *Computer Simulations of Dislocations (Oxford Series on Materials Modelling)*. Oxford University Press, dec 2006.

[5] Lisa Ventelon, B. Lüthi, E. Clouet, L. Proville, B. Legrand, D. Rodney, and F. Willaime. Dislocation core reconstruction induced by carbon segregation in bcc iron. *Physical Review B*, 91(22), June 2015.

[6] M. Itakura, H. Kaburaki, M. Yamaguchi, and T. Okita. The effect of hydrogen atoms on the screw dislocation mobility in bcc iron: a first-principles study. *Acta Materialia*, 61(18):6857–6867, 2013.

[7] C.S. Becquart, J.M. Raulot, G. Bencteux, C. Domain, M. Perez, S. Garruchet, and H. Nguyen. Atomistic modeling of an fe system with a small concentration of c. *Computational Materials Science*, 40(1):119–129, July 2007.

[8] Emmanuel Clouet, Sébastien Garruchet, Hoang Nguyen, Michel Perez, and Charlotte S. Becquart. Dislocation interaction with c in -fe: A comparison between atomic simulations and elasticity theory. *Acta Materialia*, 56(14):3450–3460, August 2008.

[9] Y. Hanlumyuang, P.A. Gordon, T. Neeraj, and D.C. Chrzan. Interactions between carbon solutes and dislocations in bcc iron. *Acta Materialia*, 58(16):5481–5490, September 2010.

[10] Stela Makri, Christoph Ortner, and James R. Kermode. A preconditioning scheme for minimum energy path finding methods. *The Journal of Chemical Physics*, 150(9):094109, March 2019.

[11] David Rodney and Laurent Proville. Stress-dependent peierls potential: Influence on kink-pair activation. *Physical Review B*, 79(9), March 2009.